MRS Communications

https://doi.org/10.1557/s43579-024-00579-8

MRS Communications

Advanced Catalytic Materials: Nano and Bulk Research Letter

Enhancement of the CO oxidation reaction: Impact of the precursor addition sequence on the synthesis of Au-Co_3O_4/Al_2O_3 catalysts

Alexis Hellmer, Instituto de Ciencias Aplicadas y Tecnología, Universidad Nacional Autónoma de México, Circuito Exterior S/N, Cd. Universitaria, Del. Coyoacán, CP 04510 Ciudad de Mexico, Mexico
Rubén Mendoza-Cruz, Instituto de Investigaciones en Materiales, Universidad Nacional Autónoma de México, Circuito Exterior S/N, Cd. Universitaria, Del. Coyoacán, CP 04510 Ciudad de Mexico, Mexico
Rodolfo Zanella, Instituto de Ciencias Aplicadas y Tecnología, Universidad Nacional Autónoma de México, Circuito Exterior S/N, Cd. Universitaria, Del. Coyoacán, CP 04510 Ciudad de Mexico, Mexico

Address all correspondence to Rodolfo Zanella at **rodolfo.zanella@icat.unam.mx**

(Received 14 November 2023; accepted 29 May 2024)

Abstract

In the present work, it is demonstrated that a synergistic effect on the CO oxidation reaction can be achieved depending on the cobalt loading and deposition order of metal precursors employed in the synthesis of Au-Co_3O_4/Al_2O_3 catalysts by the deposition precipitation with urea method. The atomic arrangement of Au and Co_3O_4 exerts an important influence on the catalytic activity. Intermediate reaction species in the studied systems were identified through DRIFTS spectroscopy, which provided insights into the reaction mechanism. The formation of Au^0 and $Au^{\delta-}$ as active sites for CO oxidation, along with mono- and bidentate bicarbonate ligands as active reaction intermediates, was elucidated.

Introduction

It is generally accepted that the catalytic activity of gold in CO oxidation depends on its particle size, however, the type of support, preparation method, previous thermal treatment and Au-support interaction have also been found to be determining factors for the catalytic performance.[1,2] The reducibility of the support also influences the adsorption sites of reactive molecules. When gold is supported on alumina, whose participation is not considered in the catalytic process, only moderately active catalysts are obtained.[3–5] However, Au catalysts supported on reducible transition metal oxides have exhibited very high activities.[6] Grisel and Nieuwenhuys employed MO_x/Al_2O_3 mixed oxides to prepare Au/MO_x/Al_2O_3 catalysts and tested them in CO and CH_4 oxidation[5]; these transition metal oxides showed high CO oxidation activity, as well as in the selective CO oxidation reaction in the presence of H_2.[7] Au/Co_3O_4 catalysts have been studied for CO oxidation,[5,8,9] and the Au/Co_3O_4/Al_2O_3 system, synthesized by Au and Co impregnation, has been used in the oxidation of cyclohexane.[10] In this context, the deposition–precipitation (DP) method is more advantageous than the impregnation or precipitation methods, for a high percentage of gold species remain on the support surface without Cl^- residues on the catalysts, forming small particles of about 3 nm.[11] To the best of our knowledge, through the DP method, the effect of the synthesis sequence of metal precursors on the interaction between Au and Co_3O_4 supported on a non-reducible support has not been studied. Moreover, the Au/Co_3O_4/Al_2O_3 system has not been studied as catalyst for CO oxidation. Therefore, in the present research work, the deposition sequence of gold and cobalt precursors on γ-Al_2O_3 was varied to study its influence on the Au-CoO_x interaction by correlating structural and surface properties with the activity in the CO oxidation reaction.

Materials and methods

Preparation of catalysts

The catalysts were synthesized by the DP method using urea as precipitating agent. Prior to preparation, γ-Al_2O_3 (Aeroxide Alu C, 85–115 m^2g^{-1}) was dried at 100°C for 24 h to desorb any species that might be present on the surface. $HAuCl_4{\cdot}3H_2O$ (Aldrich, 99.999%) and $Co(NO_3)_2{\cdot}6H_2O$ (Aldrich) were employed as precursors of gold and cobalt, severally. The synthesis of monometallic catalysts consisted in suspending γ-Al_2O_3 in a solution of the metal precursor by basifying it (pH 8–9) with the addition and decomposition of urea. Constant stirring was maintained at 80°C for 16 h. Once this process was completed, the solid was separated from the solution by centrifugation, washed with distilled water, stirred, and heated (at 50°C) until obtaining a solution pH of around 7; then, the sample was dried in a vacuum oven at 80°C. For deposition of the metal precursor by sequential DP, a series of catalysts were synthesized by first depositing $Co(NO_3)_2$, then the sample was vacuum dried at 50ºC and afterward, the deposition of the $HAuCl_4$ precursor was conducted as described above. The obtained catalysts were labeled as $AuCo_X/Al_2O_3$, where X denotes the Au:Co molar ratio in each sample. On the other hand, another series of catalysts was synthesized by first depositing gold and then cobalt, following the same preparation methodology; in this case, the samples were labeled as

Co_XAu/Al_2O_3. The theoretical deposited gold loading was 3 wt. %, whereas that of cobalt was varied, obtaining Au:Co molar ratios of 1:1 and 1:3.

Characterization of catalysts

Elemental analysis was carried out by X-Ray energy dispersive spectroscopy (EDS) on a JEOL 5900-LV scanning electron microscope with an Oxford ISIS model EDS detector. Scanning transmission electron microscopy in high-angle annular dark-field (STEM-HAADF) mode was performed using a JEOL ARM-200F Cs-corrected electron microscope, operated at 200 kV and located at Laboratorio Universitario de Microscopía Electrónica (LUME, RRID:SCR_024400). Images of the catalysts thermally treated *ex situ* at 400°C in air flow for 2 h were acquired to determine the average particle size, setting convergence and collection semi-angles of ~25mrad and 68–260 mrad, respectively. UV–Visible spectroscopy analyses were performed in a CARY 5000 (UV–VIS-NIR) by Agilent Technologies equipped with a Praying Mantis diffuse reflectance cell and a high temperature reaction chamber. The synthesized catalysts were thermally treated *in situ* under air flow of 50 mL.min^{-1} with a heating ramp of 2°C·min^{-1} from room temperature to 350°C. Spectra were recorded during the thermal treatment every 5 min to observe the evolution of the surface plasmon resonance band (SPR). For the diffuse reflectance infrared Fourier transform spectroscopy (DRIFT) analysis, the samples were previously thermally treated *in situ* at 300°C under air flow; after cooling and purging the system with N_2, a flow rate of 50 mL·min^{-1} of CO was passed through the samples, analyzing the evolution of the spectra with respect to time, at room temperature and stabilizing the spectra for 60 min. These tests were carried out in an IR spectrophotometer (Nicolet Nexus IS50R FT-IR) equipped with a Praying Mantis cell for diffuse reflectance spectroscopy and a reaction chamber (Harrick) for high temperatures.

Catalytic test

CO oxidation catalytic tests were performed in a fixed-bed reactor, in an *in-situ* research RIG-150 coupled to an Agilent Technologies GC-7820A gas chromatograph with FID detector, using a heating ramp of 2°C min^{-1}. The reactant gas mixture was CO and O_2, both at 1 vol% balanced with N_2. A flow rate of 100 mL min^{-1} and 80 mg of catalyst were used to perform the catalytic test, which corresponded to a weight hourly space velocity (WHSV) of 187.5 h^{-1}, defined as the weight of feed flowing per unit weight of catalyst per hour.

Results and discussion

According to the elemental analysis (see Table 1 in Online Resource), the percentage of Au and Co deposited on the support was above 70% of the theoretical one, obtaining Au:Co ratios of 1:1.18 and 1:2.98 for the $AuCo_{1.18}/Al_2O_3$ and $AuCo_{2.98}/Al_2O_3$ samples; and Co:Au ratios of 1.25:1 and 3.10:1 for the $Co_{1.25}Au/Al_2O_3$ and $Co_{3.10}Au/Al_2O_3$ samples, severally.

Catalytic oxidation of CO

The results of the catalytic CO oxidation tests are shown in Fig. 1. The Au/Al_2O_3 catalyst exhibited a conversion of 49% at 0°C, while the Co/Al_2O_3 catalyst showed no activity at temperatures lower than 100°C, reaching 30% of CO conversion at 200°C. The low catalytic activity of Co/Al_2O_3 at low temperatures is attributed to kinetic barriers on the catalyst surface. Additionally, since Al_2O_3 is a non-reducible support, it cannot participate in oxygen activation through a redox mechanism. At temperatures higher than 100°C, CO oxidation on cobalt oxide may be limited by the desorption rate of CO_2, as proposed by Bridge et al.[12] Another plausible explanation is that water adsorbed on the cobalt surface forms OH groups, which reduces the activity of preoxidized cobalt catalysts.[13]

When cobalt was incorporated into the Au/Al_2O_3 catalyst to form bimetallic systems, the catalysts with 1:1 molar ratio,

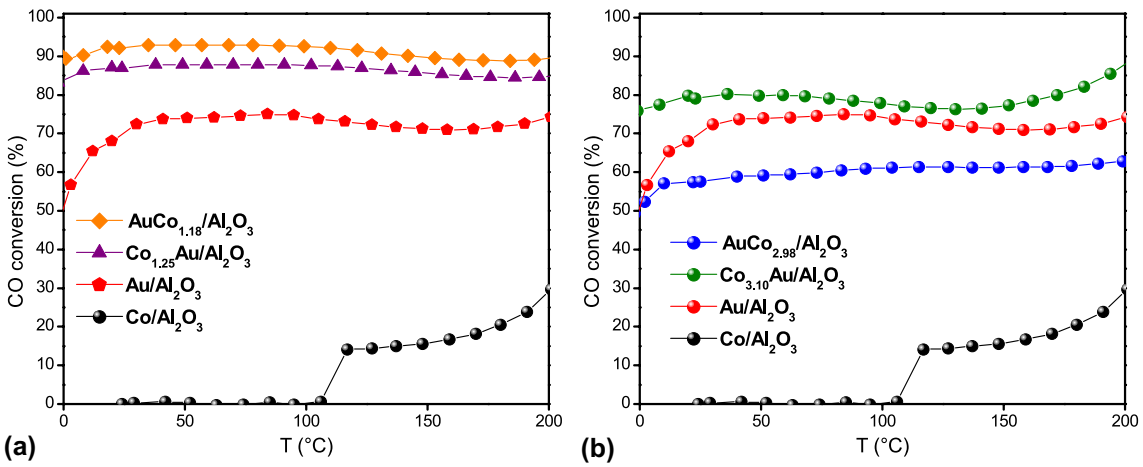

Figure 1. Light-off curves of supported Au–Co catalysts in the catalytic oxidation of CO with Au:Co molar ratios of (a) 1:1 and (b) 1:3, WHSV = 187.5 h^{-1}.

$Co_{1.25}Au/Al_2O_3$ and $AuCo_{1.18}/Al_2O_3$, showed CO conversions of 84 and 89% at 0°C, respectively. Then, the effect of the synthesis sequence was not relevant for this preparation method, since the samples displayed very similar conversion profiles with slight differences of about 5% in CO conversion. By increasing the Au:Co molar ratio to 1:3, a different behavior pattern was observed. The $Co_{3.10}Au/Al_2O_3$ sample achieved a conversion of 76% at 0°C, while by inversing the deposition sequence of the metal precursors for the $AuCo_{2.98}/Al_2O_3$ catalyst, the conversion decreased even below the one of the Au/Al_2O_3 catalyst. At 0°C, the CO conversion was 50% and below 200°C, it did not exceed 60%.

In this sense, the catalytic performance decreased with the increasing Au:Co molar ratio and the effect of the deposition sequence of the Au and Co metal precursors had notable influence on these catalysts. In the $Co_{1.25}Au/Al_2O_3$ and $AuCo_{1.18}/Al_2O_3$ samples, and to lower extent in the $Co_{3.10}Au/Al_2O_3$ sample, a promoting effect on the catalytic activity was observed.

It should be noted that the CO conversion profiles as a function of the reaction temperature are characteristic of gold catalysts supported on alumina; this behavior, in which the CO conversion presents an apparent decrease, above 50°C, is due to the possible loss of active sites. Costello et al.[14] demonstrated that when Al_2O_3 is used, Au^+–OH^- species are involved in the CO oxidation reaction. These authors proposed a reaction mechanism involving the insertion of CO into Au^+–OH^- to form gold hydroxycarbonyls, Au–(CO_3H), that are oxidized to bicarbonates, which decompose into CO_2, releasing the Au-hydroxyl site to complete the reaction cycle. However, inactive Au–CO_3–Al carbonates and H_2O can also be formed by dehydration of Au–(CO_3H) + Al–OH, which may explain the catalyst deactivation.[15]

Size and formation of Au and Au–Co nanoparticles

STEM-HAADF micrographs of bimetallic samples are shown in Fig. 2. It was observed that by increasing the molar ratio in the samples where cobalt was first deposited, $AuCo_{1.18}/Al_2O_3$ and $AuCo_{2.98}/Al_2O_3$ catalysts, the particle size decreased considerably from 4.27 to 2.67 nm, respectively (see histograms in Fig. 1 in Online Resource). This agrees with the literature, where it is generally reported that gold nanoparticles deposited on a reducible oxide are more stable against agglomeration.[16] In the samples where gold was first deposited, Co_xAu, the particle diameter remained around 3.15 nm, which is the same size obtained for the Au/Al_2O_3 catalyst, see Fig. 1 in Online Resource. In fact, 70% of the particles showed diameters between 2 and 3 nm in the $AuCo_{2.98}/Al_2O_3$ catalyst, while 63% of the particles displayed diameters between 3 and 4 nm in the $Co_{3.10}Au/Al_2O_3$ catalyst, which is in contrast with 55% of the gold nanoparticles that reached diameters between 2.5 and 3.5 nm in the Au/Al_2O_3 sample.

A synergistic effect on the CO oxidation reaction was observed for the bimetallic samples, suggesting an interaction between Au and Co_3O_4 in the nanoparticles. To support this idea, high-magnification HAADF images were acquired for the $AuCo_{1.18}/Al_2O_3$ and $Co_{3.10}Au/Al_2O_3$ catalysts. In both cases, the particles showed contrast variations within their structure attributable to differences in composition in these areas. This fact indicates that the particles consist of Au (higher contrast) and Co (lower contrast), sharing an interface as highlighted by the yellow arrows in Figs. 2(e), (i), (j). The $AuCo_{1.18}/Al_2O_3$ particle in Fig. 2(g) shows a lattice pattern that differs from that of Au, particularly in the Co-rich area. The fast Fourier transform (FFT) of the image displayed a [112]-like pattern, characteristic of a face-centered cubic structure (highlighted in golden color). The reflections at 142 and 238 pm matched the $(2\bar{2}0)_{Au}/(4\bar{4}0)_{Co3O4}$ and $(11\bar{1})_{Au}/(2\bar{2}\bar{2})_{Co3O4}$ planes. The reflections at 470 pm and 245 pm (indicated by white arrows) matched the $(11\bar{1})$ and $(3\bar{1}\bar{1})$ planes of the Co_3O_4 phase. In the $Co_{3.10}Au/Al_2O_3$ sample, the contrast difference within the particle increased due to higher Co content, with particles crystallizing with more irregular shape. The FFT in Fig. 2(k) once again shows an additional reflection at 248 pm, corresponding to the {311} planes of the Co_3O_4 phase. To further confirm the presence of cobalt within the structure of particles, EDS line scans along single particles were carried out and plotted in Fig. 2(h), (l). As observed, the particles showed the presence of cobalt in a minor proportion than gold, with the cobalt signal appearing in the low-contrast areas of the NP. HAADF imaging and line scan analysis suggested an interaction between Au and Co/Co_3O_4 within the particles of the bimetallic samples, which may explain the promoting effect observed in some bimetallic samples.

To further analyze the formation of gold nanoparticles in the $AuCo_{2.98}/Al_2O_3$ and $Co_{3.10}Au/Al_2O_3$ catalysts, where important influence of the synthesis sequence on the catalytic behavior was observed, the evolution of the SPR gold bands were analyzed during the *in-situ* thermal treatment under air flow, comparing them with their monometallic counterparts, see Fig. 3. In the bimetallic samples, the appearance of three absorption bands was observed: two corresponding to Co_3O_4 bands that confirmed the presence of the cobalt oxide spinel, found at 410 and 710 nm due to $O^{2-} \rightarrow Co^{2+}$ and $O^{2-} \rightarrow Co^{3+}$ charge transfer,[17,18] respectively, and a band at 520 nm characteristic of the reduction of Au^{3+} to form metallic gold nanoparticles. Unlike the evolution of the Au band in the Au/Al_2O_3 catalyst, where the formation of a plasmon band was observed from 250°C, in the $AuCo_{2.98}/Al_2O_3$ and $Co_{3.10}Au/Al_2O_3$ catalysts, SPR was detected at 210°C and its intensity increased gradually as the temperature increased. This difference in the evolution of the plasmon band may stem from the interaction between Au and Co_3O_4 in these samples.

Besides, the decrease in the intensity of the absorption band of gold particles in the $AuCo_{2.98}/Al_2O_3$ catalyst could be due to the Au–Co interaction in the particles, which has been associated with plasmon suppression.[19,20] This interaction could be due to a partial or total coverage of the gold nanoparticles by Co_3O_4, which prevented their growth. In fact, the $AuCo_{2.98}/Al_2O_3$ catalyst presented both the lowest particle size

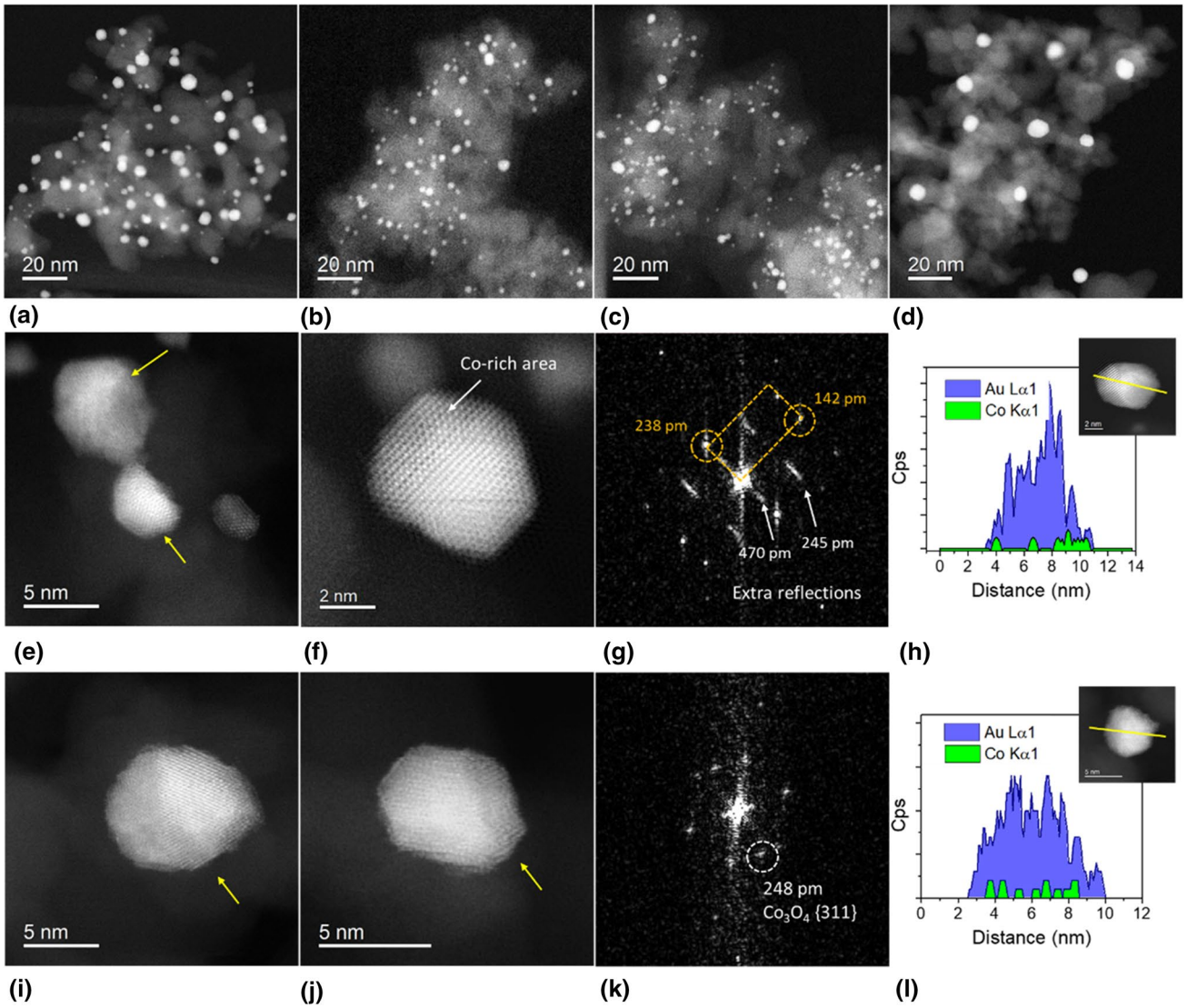

Figure 2. HAADF TEM images of samples (a) $AuCo_{1.18}/Al_2O_3$, (b) $Co_{1.25}Au/Al_2O_3$, (c) $AuCo_{2.98}/Al_2O_3$, and (d) $Co_{3.10}Au/Al_2O_3$ thermally treated at 400°C in air. (e), (f) High-magnification images of single $AuCo_{1.18}/Al_2O_3$ particles. (g) FFT of image in panel f. Extra reflections correspond to Co_3O_4 planes formed in the Co-rich side of the particle. The Au symmetry is indicated by the yellow square. (h) EDS line scan across a single particle showing the presence of Au and Co in its structure. (i), (j) High-magnification images of single $Co_{3.10}Au/Al_2O_3$ particles. A clear interface between high and low contrast is formed by the difference in atomic number between Au and Co, pointed out by arrows. (k) FFT of image in panel k. The distance of 248 pm corresponds to the {311} planes of Co_3O_4. (l) EDS line scan across a single particle showing the presence of Au and Co in its structure.

of 2.67 nm and the lowest catalytic performance, which is in line with the proposal that gold is at least partially covered by Co species.

Surface characterization

Surface analysis with DRIFT spectroscopy was performed to elucidate the possible active sites in the synthesized catalysts and the possible intermediate species. Figure 4 shows the spectra obtained after saturating the surface by flowing CO for 60 min at 25°C. The bands at 2167 and 2122 cm^{-1} are attributed to adsorbed CO on Au species,[21,22] while the band at 2167 cm^{-1} has also been associated with the adsorption of CO on Au^{+n}.[23] This last species is related to active sites for the catalytic oxidation of CO with the formation of Au^{+}–OH^{-} (OH^{-} groups coming from alumina).[24,25] However, this peak has also been observed in Co/Al_2O_3 catalyst DRIFT spectra, so it is more likely that the band at 2167 cm^{-1} corresponds to the contribution of CO in the gas phase. The band appearing at 2101 cm^{-1} corresponds to the adsorption of CO on metallic Au[23]; this adsorption band occurred with similar intensity for the Au/Al_2O_3, $AuCo_{1.18}/Al_2O_3$ and $Co_{3.10}Au/Al_2O_3$ catalysts. According to Boccuzzi et al.[26], CO is adsorbed on step-like defects of the metal particles and the higher intensity of this CO vibrational frequency indicates higher number of

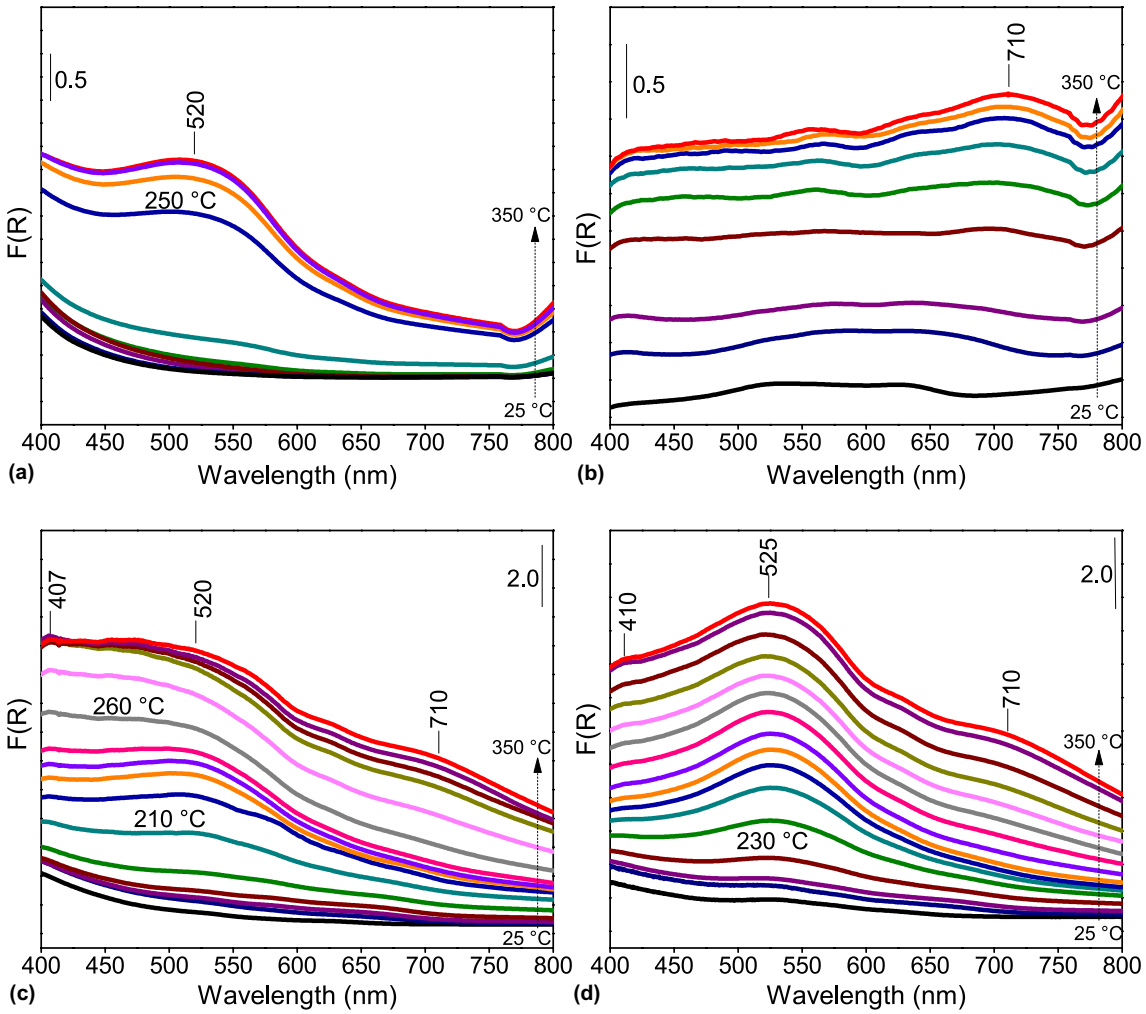

Figure 3. UV–Vis absorption spectra for (a) Au/Al_2O_3, (b) Co/Al_2O_3, (c) $AuCo_{2.98}/Al_2O_3$ and (d) $Co_{3.10}Au/Al_2O_3$ thermally treated *in situ* under air atmosphere.

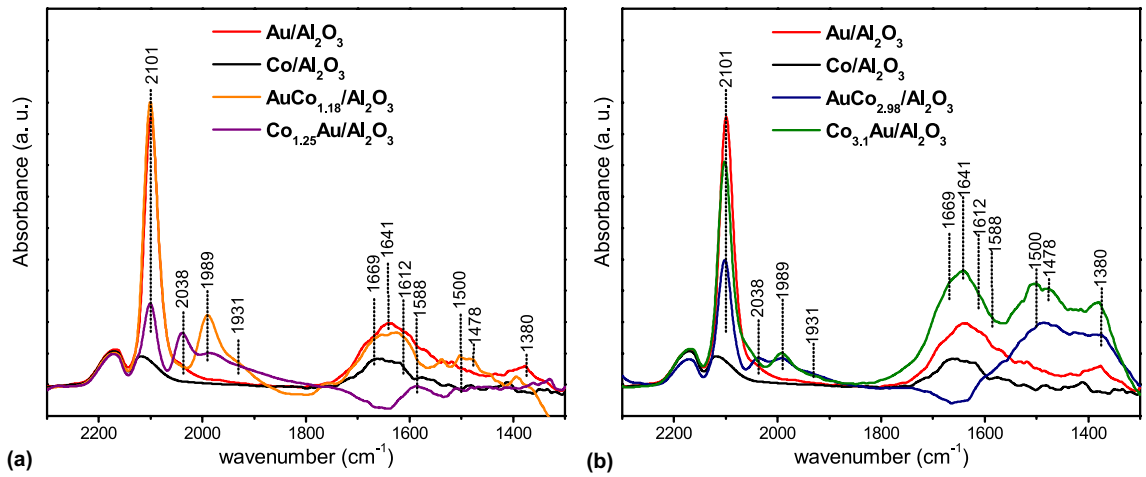

Figure 4. Diffuse reflectance Fourier transform infrared spectroscopy (DRIFTS) of the samples with Au:Co molar ratio of (a) 1:1 and (b) 1:3, thermally treated at 400°C in air.

Au^0 active sites. Moreover, it was observed that this band in the spectra of the $AuCo_{2.98}/Al_2O_3$ and $Co_{1.25}Au/Al_2O_3$ catalysts presented low intensity, indicating lower availability of metallic gold species which would confirm that gold could be partially covered by cobalt oxide in the $AuCo_{2.98}/Al_2O_3$ sample, which is also in line with their catalytic performance that was lower than that displayed by the $AuCo_{1.18}/Al_2O_3$ and $Co_{3.10}Au/Al_2O_3$ samples.

The band appearing at 2038 cm^{-1} along with a shoulder at 1989 cm^{-1} correspond to CO adsorption on $Au^{\delta-}$[27,28] and were present in the $AuCo_{2.98}/Al_2O_3$ and $Co_{1.25}Au/Al_2O_3$ catalysts. In the $AuCo_{1.18}/Al_2O_3$ and $Co_{3.10}Au/Al_2O_3$ samples, a shift to low frequencies of these bands occurred at 1989 and 1931 cm^{-1}. The intensity of these bands was higher for catalysts with Au:Co molar ratio of 1:1. This band is formed according to the conversion of CO–Au^0 to CO–$Au^{\delta-}$ sites by redox equilibrium due to charge transfer. The appearance of these bands between 2038 and 1931 cm^{-1} indicates different CO–$Au^{\delta-}$ species with different transferred electron density.[28] These negatively charged sites on gold nanoparticles may also be due to their interaction with Co_3O_4, oxygen vacancies, because CO adsorption modifies the electron density around the CO–Au–Co_3O_4 adsorption sites. Chakarova et al. reported that negatively charged gold species, exhibiting strong metallic character, successfully adsorbed the CO molecule, which produced the weakening of the C–O bond by metal–CO bonding effect and promoted the formation of carbonates as reaction intermediates. The above facts could explain the bands in the carbonate region, between 1700 and 1550 cm^{-1}, observed in the spectra of the $AuCo_{1.18}/Al_2O_3$, $Co_{3.10}Au/Al_2O_3$ and Au/Al_2O_3 catalysts.

The bands at 1669, 1641, 1612 and 1588 cm^{-1} are associated with the adsorption of bidentate COOH, bi- and monodentate bicarbonates and bidentate CO on Au,[29] severally; they were observed with higher intensity with the Au/Al_2O_3, $AuCo_{1.18}/Al_2O_3$ and $Co_{3.10}Au/Al_2O_3$ catalysts, but these peaks were not observed with the $AuCo_{2.98}/Al_2O_3$ and $Co_{1.25}Au/Al_2O_3$ catalysts. On the other hand, the bands with higher intensity at 1500, 1478 and 1380 cm^{-1} correspond to the adsorption of HCOO and COOO on either Au or on the support, to either monodentate carbonate or free carbonate and symmetric stretch vibrations of different carbonates and of formate species, respectively;[21,30] these adsorbed species were identified on the catalysts with Au:Co molar ratio of 1:3.

The band at 1641 cm^{-1} is related to the formation of $Au^{\delta-}$ species and the adsorption of bidentate bicarbonates; the presence of this band is also correlated with the catalytic performance shown by the $AuCo_{1.18}/Al_2O_3$ catalyst, which had the highest CO conversion at 0°C. These results agree with what was reported by Costello et al.,[14] who proposed that the presence of these negatively charged gold species promoted the formation of bicarbonates, which are considered as reaction intermediates. As for the $Co_{3.10}Au/Al_2O_3$ catalyst, the band at 1641 cm^{-1} appeared with high intensity, however, the bands corresponding to the adsorption of HCOO and COOO also displayed high intensity, as well as in the DRIFT spectra of the $AuCo_{2.98}/Al_2O_3$ sample, which could be related to the formation of inactive carbonates. The foregoing observations are in line with the proposal stating that a smaller number of gold active sites are available on the surface of these catalysts with cobalt species as the prevailing ones. The aforementioned would explain the decrease of the catalytic performance in the catalysts with Au:Co molar ratio of 1:3. A schematic representation of the possible catalytic reaction mechanism taking place over these particles can be seen in Fig. 2 in the Online Resource.

The effect of the synthesis sequence was mainly observed through the formation of nanoparticles enriched in either Au or Co on their surface. This fact suggests that gold availability on the catalytic surface varied, exerting a significant influence on the catalytic activity. This phenomenon promoted the formation of bicarbonates as reaction intermediates and inactive carbonates or spectators. The catalysts with larger particle size, $Co_{3.10}Au/Al_2O_3$ and $AuCo_{1.18}/Al_2O_3$, exhibited the formation of bidentate bicarbonates.

Conclusions

The CO oxidation conversion shown by the synthesized catalysts followed the order: $AuCo_{1.18}/Al_2O_3 > Co_{1.25}Au/Al_2O_3 > Co_{3.10}Au/Al_2O_3 > Au/Al_2O_3 > AuCo_{2.98}/Al_2O_3$. The catalytic performance was influenced by the effect of the deposition sequence of the metal precursors on Al_2O_3, which impacted the formation stability of gold nanoparticles. As the cobalt loading increased in the catalysts where cobalt was first deposited, the size of the gold nanoparticles decreased, while in the catalysts where gold was first deposited, the particle size did not undergo a significant change. Furthermore, the addition of Co_3O_4 promoted the formation of active sites in $Au^{\delta-}$ species. However, when the cobalt loading was increased, gold particles were, apparently, partially covered by Co species, decreasing the Au^0 and $Au^{\delta-}$ species available on the surface and promoting an increase in the formation of HCOO and COOO that are considered as spectators in the reaction mechanism, which implies a decrease in available active sites and therefore, a decrease in the catalytic performance.

Acknowledgments

The authors want to thank the financial support provided by the Consejo Nacional de Humanidades, Ciencias y Tecnologías (CONAHCYT) through the CB A1-S-18269 grant, Dirección General de Asuntos del Personal Académico-UNAM through the PAPIIT IN104022 and IA106623 grants. A. Hellmer is a doctoral student at the Programa de Maestría y Doctorado en Ingeniería, Universidad Nacional Autónoma de México (UNAM), and gratefully acknowledges the fellowship 921722 granted by CONAHCYT.

Author contributions

Alexis Hellmer: Investigation, methodology, formal analysis, conceptualization, writing—original draft preparation. Rubén Mendoza-Cruz: Methodology, formal analysis. Rodolfo Zanella: Supervision, conceptualization, formal analysis, funding acquisition, writing—review & editing.

Funding

Consejo Nacional de Humanidades, Ciencias y Tecnologías (CONAHCyT) through the CB A1-S-18269 grant, and PhD fellowship 921722 granted to Alexis Hellmer; Dirección General de Asuntos del Personal Académico-UNAM through the PAPIIT IN104022 grant.

Data availability

Data will be made available on request.

Declarations

Conflict of interest

On behalf of all the authors, the corresponding author states that there is no conflict of interest.

Supplementary Information

The online version contains supplementary material available at https://doi.org/10.1557/s43579-024-00579-8.

Open Access

References

1. M. Haruta, Catal. Today **36**, 153–166 (1997)
2. N. Lopez, T.V.W. Janssens, B.S. Clausen, Y. Xu, M. Mavrikakis, T. Bligaard, J.K. Norskov, J. Catal. **223**, 232 (2004)
3. D. Gavril, A. Georgak, V. Loukopoulos, G. Karaiskakis, B.E. Nieuwenhuys, Gold Bull. **39**, 192–199 (2006)
4. E. Quinet, F. Morfin, F. Diehl, P. Avenier, V. Caps, J.L. Rousset, Appl. Catal. B **80**, 195–201 (2008)
5. R.J.H. Grisel, B.E. Nieuwenhuys, Catal. Today **64**, 69–81 (2001)
6. M.M. Schubert, S. Hackenberg, A.C. van Veen, M. Muhler, V. Plzak, R.J. Behm, J. Catal. **197**, 113–122 (2001)
7. R.J.H. Grisel, B.E. Nieuwenhuys, J. Catal. **199**, 48–59 (2001)
8. D.A.H. Cunningham, T. Kobayashi, N. Kamijo, M. Haruta, Catal. Lett. **25**, 257–264 (1994)
9. M. Haruta, S. Tsubota, T. Kobayashi, H. Kageyama, M.J. Genet, B. Delmon, J. Catal. **144**, 175 (1993)
10. J. Zhao, M.Q. Zhu, J.J. Chen, Y.Y. Yang, Y. Tang, Z. Cai, Y.Y. Shen, C.H. He, Adv. Mater. Res. **233–1**, 254–259 (2011)
11. F. Boccuzzi, A. Chlorino, S. Tsubota, M. Haruta, J. Phys. Chem. **100**, 3625–3631 (1996)
12. M.E. Bridge, R.M. Lambert, Surf. Sci. **82**, 413 (1979)
13. F.F. Ma, S.H. Ma, Z.Y. Jiao, X.Q. Dai, Appl. Surf. Sci. **384**, 10–17 (2016)
14. C.K. Costello, J.H. Yang, H.Y. Law, Y. Wang, J.N. Lin, L.D. Marks, M.C. Kung, H.H. Kung, Appl. Catal. A: Gen. **243**, 15–24 (2003)
15. C.K. Costello, M.C. Kung, H.-S. Oh, Y. Wang, H.H. Kung, Appl. Catal. A Gen. **232**, 159 (2002)
16. Y.W. Chen, H.J. Chen, D.S. Lee, J. Mol. Catal. A: Chem. **363**, 470–480 (2012)
17. S. Kandula, P. Jeevanandam, RSC Adv. **5**, 5295–5306 (2015)
18. B. Richa, K. Shakeel, A. Naseem, A.I.P. Conf, Proc. **1953**, 030034 (2018)
19. M.G. Blaber, M.D. Arnold, M.J. Ford, J. Phys. Condens. Matter **22**, 143201 (2010)
20. V. Amendola, R. Pilot, M. Frasconi, O.M. Marago, M.A. Lati, J. Phys. Condens. Matter **29**, 203002 (2017)
21. B. Schumacher, Y. Denkwitz, V. Plzak, M. Kinne, R.J. Behm, J. Catal. **224**, 449–462 (2004)
22. L. Piccolo, H. Daly, A. Valcarcel, F.C. Meunier, Appl. Catal. B: Env. **86**, 190–195 (2009)
23. M.A. Centeno, K. Hadjiivanov, T. Venkov, H. Klimev, J.A. Odriozola, J. Mol. Catal. A: Chem. **252**, 142–149 (2006)
24. M.C. Kung, R.J. Davis, H.H. Kung, J. Phys. Chem. C **111**, 11767–11775 (2007)
25. A. Leba, T. Davran-Candan, Z.I. Önsan, R. Yildirim, Catal. Commun. **29**, 6–10 (2012)
26. F. Boccuzzi, A. Chorino, Stud. Surf. Sci. Catal. **140**, 77 (2001)
27. D.A. Panayotov, J.R. Morris, Surf. Sci. Rep. **71**, 77–271 (2016)
28. K. Chakarova, M. Mihaylov, S. Ivanova, M.A. Centeno, K. Hadjiivanov, J. Phys. Chem. C **115**, 21273–21282 (2011)
29. M.C. Raphulu, J. McPherson, E. van der Lingen, J.A. Anderson, M.S. Scurrell, Gold Bull. **43**, 21 (2010)
30. S. Gaur, H. Wu, G.G. Stanley, K. More, C.S.S.R. Kumar, J.J. Spivey, Catal. Today **208**, 72–81 (2013)